Journal of Molecular Graphics and Modelling 135 (2025) 108913

Contents lists available at ScienceDirect

Journal of Molecular Graphics and Modelling

journal homepage: www.elsevier.com/locate/jmgm

A novel *in silico* approach for identifying multi-target JAK/STAT inhibitors as anticancer agents

Alessia Bono [a], Gabriele La Monica [a], Federica Alamia [a], Antonino Lauria [a,b,*], Annamaria Martorana [a]

[a] Dipartimento di Scienze e Tecnologie Biologiche Chimiche e Farmaceutiche "STEBICEF" – University of Palermo, Viale delle Scienze – Ed. 17, 90128, Palermo, Italy
[b] NBFC, National Biodiversity Future Center, Piazza Marina 61, Palermo, 90133, Italy

ARTICLE INFO

Keywords:
Apoptosis
Inhibitors
OFF-Targets
JAK2
JAK3
STAT3

ABSTRACT

Apoptosis, or programmed cell death, plays a pivotal role in maintaining cellular homeostasis by eliminating damaged or surplus cells. Dysregulation of signaling pathways, such as JAK/STAT, is implicated in various diseases, rendering them attractive therapeutic targets for potential new anticancer drugs. Concurrently, it is imperative to preserve essential proteins like TNF-α and p53 to maintain normal cellular life/death balance. In light of these considerations, this study employs an innovative *in silico* hybrid and hierarchical virtual screening approach aimed at identifying JAK/STAT multi-target inhibitors as potential anticancer agents for several tumoral diseases. Initially, the Biotarget Predictor Tool is utilized in a combined ON/OFF-target/Multitarget mode using the extensive National Cancer Institute (NCI) database, previously filtered by ADME evaluation tools. Subsequently, Molecular Docking studies are conducted on JAK2, JAK3, and STAT3, facilitating the identification of the most promising compound, **755435**. Finally, Molecular Dynamics Simulations validate the high stability of the potential multitarget inhibitor **755435** in complex with JAK2, JAK3, and STAT3.

1. Introduction

Apoptosis, also referred to as programmed cell death, is a tightly regulated physiological process occurring in multicellular organisms. Its primary function is to maintain cellular homeostasis by eliminating damaged or surplus cells. Additionally, apoptosis acts as a crucial defense mechanism against immune responses and contributes to the clearance of cells damaged after disease [1]. During apoptosis, cells cease their growth and division, initiating a meticulously orchestrated pathway toward cell death, often likened to "cellular suicide" [2]. This process can be instigated either by the cell itself through intracellular sensors, termed the intrinsic pathway, or by external *stimuli* triggering the extrinsic pathway, involving interactions between immune system cells and damaged cells.

The extrinsic pathway operates through death receptors located on the cell surface, such as Fas receptors, Death Receptor 4 and 5 (DR4 and DR5), Tumor Necrosis Factor Receptors (TNF), and TNF-related apoptosis-inducing ligand (TRAIL). Activation of these receptors by external signals leads to the recruitment of downstream caspase-8 and subsequent initiation of cell death processes [2,3]. Internally, stimuli like DNA damage or oxidative stress can activate the intrinsic/mitochondrial pathway of apoptosis. Within this pathway, B-cell lymphoma (Bcl) proteins, such as Bcl-2-associated X protein (BAX) and Bcl-2, regulate the release of other Bcl family members. This process culminates in the formation of the apoptosome, involving Apoptotic Protease Activating Factor-1 (APAF1) and procaspase 9, ultimately activating executioner caspases 3, 6, and 7, thus driving cell apoptosis [3].

Hence, apoptosis intricately intertwines with various signaling pathways, among which the Janus kinase/Signal Transducer and Activator of Transcription (JAK/STAT) pathway stands out as a pivotal player, primarily involved in extrinsic cellular processes such as immune modulation and hematopoiesis. Although traditionally recognized for regulating responses to extracellular signals, recent research indicates its involvement in modulating the intrinsic pathway of apoptosis. JAKs, closely associated with cytokine receptors, facilitate receptor tyrosine phosphorylation and recruit signal transducer and activator of transcription (STAT) proteins. Upon phosphorylation, STAT proteins form

* Corresponding author. Dipartimento di Scienze e Tecnologie Biologiche Chimiche e Farmaceutiche "STEBICEF" – University of Palermo, Viale delle Scienze – Ed. 17, 90128, Palermo, Italy.
E-mail address: antonino.lauria@unipa.it (A. Lauria).

https://doi.org/10.1016/j.jmgm.2024.108913
Received 5 June 2024; Received in revised form 11 October 2024; Accepted 21 November 2024
Available online 23 November 2024

dimers that translocate into the nucleus, thereby influencing gene expression. This intricate interplay underscores the JAK/STAT pathway's potential role as a regulator bridging both intrinsic and extrinsic apoptotic pathways, thereby emphasizing its multifaceted involvement in determining cellular fate [4]. The JAK-STAT pathway is tightly regulated, and any disruption in this controlled process can profoundly impact normal physiology. Mounting evidence suggests constitutive activation of JAKs in various cancers, including Acute Lymphoid Leukemia (ALL), Chronic Myelogenous Leukemia (CML), Myeloproliferative Neoplasia (MPN), lymphomas, and myelomas. Additionally, constitutively active JAKs have been implicated in solid cancers such as breast, prostate, head, and neck cancers [5–10].

The JAK family encompasses four primary members: JAK1, JAK2, JAK3, and TYK2. JAK2 and JAK3 serve as pivotal kinases in cytokine and hormone signaling pathways, playing essential roles in cytokine receptor signaling. While JAK2 is expressed ubiquitously throughout various tissues, JAK3 expression is confined to myeloid and lymphoid tissues [4,11]. Structurally, JAKs feature an N-terminal FERM domain responsible for their association with cytokine receptors, with implications for intracellular regulation of JAK activity [12]. The SH2-like domain, while not functioning as a conventional phosphotyrosine-binding domain, has a yet unclear but presumably significant role. The JH1 domain, activated via trans-phosphorylation of tandem tyrosines in the activation loop, encodes a kinase crucial for phosphorylating key substrates. Conversely, JH2, also termed the pseudokinase domain lacking kinase activity, regulates JH1 activity [13].

The activity of JAK2 undergoes tight regulation through the phosphorylation of approximately 20 tyrosine residues, which are identified as phosphorylation sites during cytokine stimulation. Among these sites, several have been functionally characterized. Notably, the activation loop, present in all JAKs and comprising tandem tyrosine residues (Tyr^{1007}-Tyr^{1008} in JAK2, and Tyr^{980}-Tyr^{981} in JAK3), serves as the primary site of autophosphorylation. Its phosphorylation is a crucial prerequisite for catalytic activation [5].

STAT3 plays a pivotal role in regulating numerous genes involved in proliferation, differentiation, apoptosis, autoimmune-inflammatory processes, and cell survival [14]. These responses are orchestrated through phosphorylation of the STAT3 SH2 domain by Janus kinases (JAKs) [15,16]. Moreover, STAT3 is frequently activated in human cancers and is implicated in regulating cancer cell survival, proliferation, angiogenesis, and metastasis [17–19], rendering it a promising target for anticancer therapies [20], particularly through approaches aimed at inhibiting STAT3 dimerization [7].

From a structural perspective, STAT3 comprises six domains: the N-Terminal Domain (NTD), Coiled-Coil Domain (CC), DNA Binding Domain (DBD), Linker Domain (LD), Src Homology 2 Domain (SH2), and Transactivation Domain (TAD) (see Fig. 1). Canonical activation of STAT3 relies on the phosphorylation of Tyr^{705}, a critical tyrosine residue, which induces SH2 domain-mediated dimerization [20]. This dimerization is further strengthened by the TAD through additional protein-protein interactions between the two monomers [21,22].

As previously mentioned, dysregulation of the JAK/STAT pathway is linked to various pathologies, warranting the use of JAK/STAT inhibitors as a compelling strategy due to the pivotal roles these proteins play in promoting oncogenesis and tumor progression. Targeting STAT3 and JAKs offers several advantages in cancer therapy. Inhibiting these proteins can disrupt signaling cascades supporting cancer cell survival, proliferation, and immune evasion. Moreover, their aberrant activation often correlates with treatment resistance, making them attractive targets for overcoming therapeutic challenges. First-generation JAK inhibitors (such as ***tofacitinib***, ***oclacitinib***, ***baricitinib***, and ***ruxolitinib***) competitively inhibit adenosine triphosphate (ATP) binding, targeting the active conformation of the JH1 tyrosine kinase domain. However, these inhibitors lack specificity, affecting various Janus kinase isoforms. In contrast, new-generation inhibitors exhibit greater selectivity and specificity, enhancing safety profiles with fewer side effects by targeting single Janus kinase isoforms [23]. JAK inhibitors can impede STAT phosphorylation and activation, yet it's crucial to note their potential interference with other signaling pathways upstream of tyrosine kinases. This interference may contribute to adverse events, prompting exploration of STAT inhibitors as a potentially more specific option with fewer side effects. Most inhibitors focus on limiting STAT phosphorylation and/or dimerization, employing peptidomimetic approaches. Alternative methods include non-peptidic small molecules and STAT inhibitors based on oligonucleotides specific to the STAT DNA-binding domain [5].

Simultaneously, p53 and TNF-α, integral components of the cellular

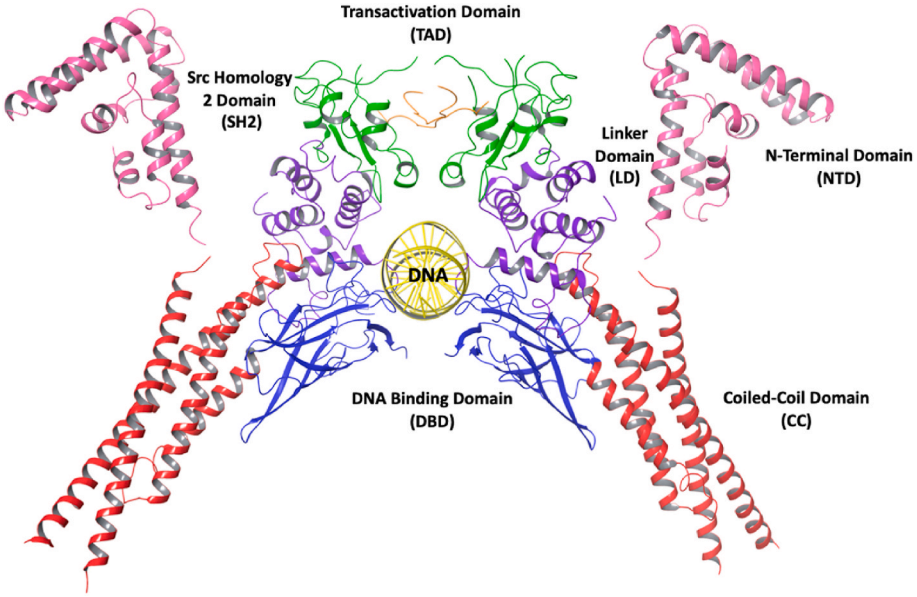

Fig. 1. 3D structure of STAT3 bounded to DNA. In detail, NTD, CC, DBD, LD, SH2, TAD, and DNA are depicted in pink, red, blue, violet, green, orange, and yellow, respectively. X-ray structures used for the image are 4ZIA for the NTD, and 6QHD for the rest of the protein. (For interpretation of the references to colour in this figure legend, the reader is referred to the Web version of this article.)

regulatory network, emerge as potential off-targets when considering interventions aimed at modulating apoptosis [24–27]. The multifaceted roles of p53 and TNF-α in orchestrating programmed cell death underscore their significance as regulators of apoptosis [28]. While activation of these molecules can enhance apoptosis and aid in the elimination of damaged cells, inhibiting them may disrupt this delicate balance, potentially impeding the natural apoptotic process. Understanding the interplay between p53, TNF-α, and apoptosis regulation provides valuable insights into the potential unintended consequences of targeting these molecules [29]. While selectively modulating them holds promise for therapeutic interventions, it becomes imperative to navigate the complexities of these pathways cautiously. Precise control over these off-target effects is essential to harness therapeutic potential while minimizing unintended consequences, ensuring a nuanced approach towards apoptosis regulation in various pathological contexts.

In light of these considerations, this study utilized an innovative *in silico* hybrid and hierarchical virtual screening approach to identify new JAK/STAT inhibitors without binding affinity against the OFF-targets p53 and TNF-α. Leveraging our in-house ligand-based Biotarget Predictor Tool (BPT) in a combined ON/OFF-targets/Multitarget mode enabled rapid screening of a large database of active molecules, previously curated, which were further scrutinized through structure-based studies.

2. Results and discussion

2.1. Database preparation

Prior to implementing the virtual screening protocol, we conducted a preliminary cleaning phase on the National Cancer Institute (NCI) database, consisting of two consecutive steps to select small molecules meeting specific parameters and requirements. Initially, the NCI database, comprising approximately 40,000 compounds analyzed by the National Cancer Institute in *in vitro* antiproliferative assays against 60 cancer cell lines (NCI60), underwent preparation using the LigPrep tool from the Schrödinger Maestro Suite, at physiological pH ($7.3 \leq pH \leq 7.5$). This process generated all possible tautomers and stereoisomers at the lowest energy state for each ligand. Subsequently, the ligands underwent analysis with the QikProp tool [30], which predicts the ADME (Absorption, Distribution, Metabolism, and Excretion) properties of drug candidates based on their full 3D molecular structure. QikProp can calculate a wide variety of pharmaceutically relevant properties, including octanol/water and water/gas partition coefficients, aqueous solubility, brain/blood partition coefficient, overall Central Nervous System (CNS) activity, Caco-2 and MDCK cell permeabilities, and log Khsa for human serum albumin binding. This process enabled rapid screening of compound libraries for potential hits.

In our study, we honed in on two specific parameters: the “Rule of Five,” indicating the number of violations of Lipinski’s rule, and "#stars," which consolidates all QikProp parameters into a single metric, representing the number of property or descriptor values that fall outside the 95 % range of similar values for known drugs. A higher number of outlying descriptors results in a higher "#stars" value, suggesting that a molecule is less drug-like compared to one with fewer "#stars". To isolate only drug-like small molecules, we discarded ligands with Rule of Five and #stars values other than 0, thereby reducing the NCI database to 18,510 compounds (see Supplementary Material, Databases S1, S2).

Considering that a significant portion of drug candidates fail in clinical trials due to poor ADME properties, integrating their predictions into the development process can yield lead compounds with satisfactory ADME performance during clinical trials. This approach contemporaneously reduces the amount of wasted time and resources while streamlining the overall development process.

To further ascertain the drug-like nature of our investigated compounds, we conducted an additional analysis using the SwissADME website (http://www.swissadme.ch, accessed on April 08, 2024 [31]). This platform enabled us to compute physicochemical descriptors and predict ADME parameters, pharmacokinetic properties, and medicinal chemistry friendliness of our screened small molecules. Specifically, a comprehensive array of parameters was predicted, including the number of heavy atoms, H-bond acceptors, H-bond donors, and rotatable bonds, as well as adherence to the Rule of Five, Blood Brain Barrier (BBB) permeability, metabolic reactions, and Human Oral Absorption—parameters shared with QikProp. Additionally, novel issues were investigated for the first time for our compounds, such as Ghose, Veber, Egan, Muegge, and lead-likeness violations, bioavailability score, and PAINS alerts. Through this analysis, we chose to retain only ligands with a PAINS alert value of 0. Furthermore, we removed duplicates, resulting in a refined database of 15,632 drug-like small molecules ready for further investigation using the proposed *in silico* protocol (see Supplementary Material, Database S3,S4).

2.2. Ligand based studies

The Biotarget Predictor Tool (BPT), available on the DRUDIT web platform (https://www.drudit.com, accessed on April 08, 2024) [32], is designed to predict the biological affinity of the given input structure against chosen biological targets.

Molecules with Multi-ON and minimal OFF target interactions represent a promising avenue for the development of highly effective and well-tolerated pharmaceuticals, ensuring that therapeutic interventions are precisely targeted. The BPT, as an established ligand-based protocol [33–38], has the advantage of being used also in a Multi and/or ON/OFF-target Mode to address the issue of selectivity in order to investigate drug molecules able to discriminate two or more biological targets.

2.2.1. Ligand based target templates building

In order to utilize the BPT, we initiated a preliminary phase of ligand-based template construction for both ON and OFF targets (ON targets: STAT3, JAK2, and JAK3; OFF targets: TNF-α and p53), as previously described in literature [39]. Large databases of known modulators for STAT3, JAK2, JAK3, TNF-α, and p53 were obtained from BindingDB [40], a trusted source of experimentally determined protein-ligand binding affinities, providing K_i, K_d, IC_{50}, EC_{50} values, and corresponding target information for numerous active molecules. Specifically, a threshold of activity $IC_{50} < 100$ nM was applied to select highly active inhibitors, followed by meticulous cleaning to remove duplicates. Subsequently, these inhibitor sets underwent molecular descriptor calculation using MOLDESTO (MOlecular DEScriptors TOols), our proprietary software [32], capable of generating over 1000 molecular descriptors (3D, 2D, and 1D) for each input structure. This process yielded a “Compounds vs. Molecular Descriptors” matrix for each database, from which two sequences of value pairs for each molecular descriptor (mean and standard deviation) were extracted, constituting the molecular descriptor-based target templates [32]. These templates were integrated into the DRUDIT platform, facilitating the assessment of ligand affinity against them.

2.2.2. Biotarget Predictor Tool application

Once all preliminary phases were concluded, we proceeded to submit the prepared database of drug-like small molecules to the in-house BPT, utilizing it in a comprehensive ON/OFF-targets/Multitarget Mode. Subsequently, 15,632 input structures were uploaded to the DRUDIT platform and analyzed through the BPT, using the “DAS – Drudit Affinity Score” parameter. In details, the DAS parameter is computed according to the choices for three input parameters N, Z and G. N is related to the number of dynamically selected molecular descriptors, Z represents the maximum allowed percentage of unavailable values (zeros) per molecular descriptor, and G defines the Gaussian smoothing function used to score the descriptor values.

For the calculation of DAS values, which ranges from 0 to 1, we used standard values of N, Z, and G, which means N = 500, Z = 50 %, G = a [32]. Lower values, closer to 0, indicate poor binding affinity between ligands and targets, whereas higher values, closer to 1, suggest a strong capability of compounds to interact with targets. Specifically, DAS values of structures for each target (ON/OFF targets), available in Supplementary Material, Matrix S1, were assessed collectively in the combined ON/OFF-targets/Multitarget Mode. This mode aimed to identify new JAK/STAT multitarget inhibitors with low affinity against the OFF targets TNF-α and p53. This was achieved by computing the "Multi-ON/OFF Target Score" using equation (1):

$$\text{Multi}-\frac{\text{ON}}{\text{OFF}}\text{Target Score} = \frac{DAS\chi}{DAS\gamma} \tag{1a}$$

Where DASχ is $DAS_{STAT3} \times DAS_{JAK2} \times DAS_{JAK3}$, and DAS$\gamma$ is $DAS_{TNF\text{-}\alpha} \times DAS_{p53}$.

Compounds were sorted in descending order based on the "Multi-ON/OFF Target Score", where a higher score indicated a higher DASχ, reflecting greater affinity for the ON targets STAT3, JAK2, and JAK3, and a lower DASγ, indicating reduced affinity for the OFF targets TNF-α and p53. Accordingly, the top-ranked 5 % of molecules (approximately 780 small molecules) were chosen for subsequent *in silico* structure-based analysis (Supplementary Material, Matrix S2).

2.3. Structure-based studies

Virtual screening has emerged as a highly effective strategy for discovering ligand hits and aiding lead optimization in drug discovery endeavors. Molecular Docking Studies, when combined with a ligand-based approach, offer the potential to identify small molecules likely to bind effectively to one or more high-resolution structures of protein targets. With this perspective in mind, a two-step docking virtual screening workflow was implemented to further refine the selected compounds based on their potential to interact with the binding pocket of the three ON targets, thereby assessing predicted binding affinity and interaction efficacy with key amino acids in the active sites. The initial step involves Extra Precision (XP) docking, aimed at pinpointing ligand poses that could exhibit unfavorable energies, thus filtering out false positives. Only active compounds with available poses demonstrating favorable contacts between the protein and the ligand, thereby circumventing such penalties, are selected for further analysis.

As an initial step, this phase was applied to the structures selected thus far, encompassing all three proteins (PDB codes 6NUQ, 6VGL, and 6GL9 for STAT3, JAK2, and JAK3, respectively) [41–43]. Docking grids were consequently generated, centering on the binding pockets of STAT3, JAK2, and JAK3, which encompassed all crucial amino acid residues. The residue-atom notation nearest to the center of the docking grid for each crystallographic structure is as follows: for JAK2, the residue is Val^{863} with an H-CH_2 atom ($Val^{863}CH_3$); for JAK3, the residue is Leu^{956} with an H-CH_2 atom ($Leu^{956}CH_3$); and for STAT3, the residue is

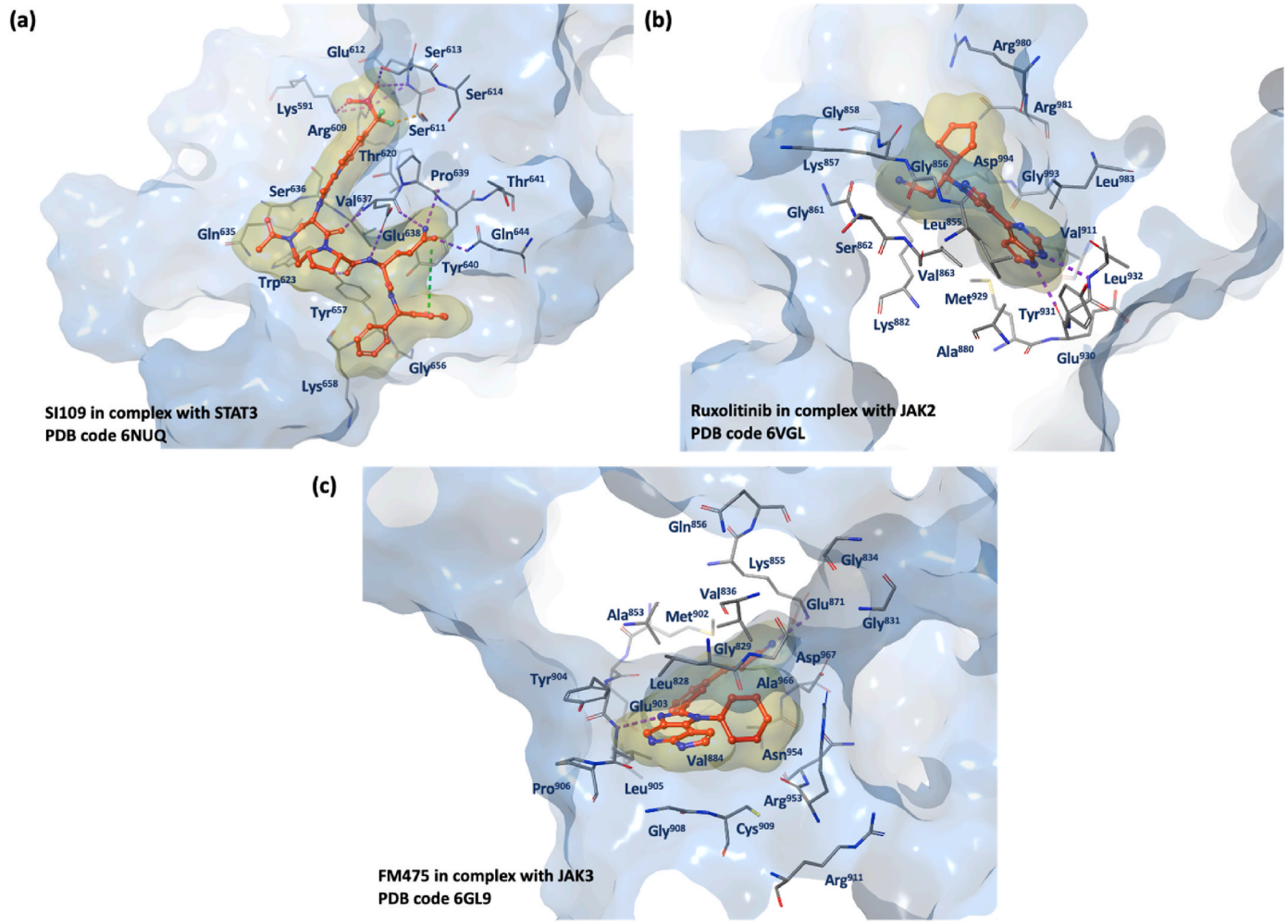

Fig. 2. **(a)** 3D x-ray structure of STAT3 SH2 Domain in complex with its co-crystalized ligand ***SI109***; **(b)** 3D x-ray structure of JAK2 JH1 Domain in complex with its co-crystalized ligand ***ruxolitinib***; **(c)** 3D x-ray structure of JAK3 JH1 Domain in complex with its co-crystalized ligand ***FM475***.

Glu^{638} with an H-N atom (Glu^{638}NH). Fig. 2a–c illustrates the 3D binding sites of STAT3 in complex with compound ***SI109*** (PDB code 6NUQ [42]), JAK2 in complex with ***ruxolitinib*** (PDB code 6VGL [41]), and JAK3 in complex with compound ***FM475*** (PDB code 6GL9 [43]).

Fig. 2a illustrates the STAT3 SH2 domain, highlighting essential components for p-Tyr^{705} recognition. These include the pivotal residue Arg^{609}, crucial for stabilizing p-Tyr^{705} via favorable electrostatic interaction energy between the negatively charged phosphate and the positively charged NH3 amino group. Additionally, residues Lys^{591}, Ser^{611}, and Ser^{613} facilitate the formation of polar interactions. Furthermore, STAT3 harbors residues susceptible to various post-translational modifications, such as Lys^{658} and Lys^{679}. Acetylation at these sites can modulate STAT3 diverse functions and properties, including protein dimerization, transcriptional activity, mitochondrial translocation, and methylation of tumor-suppressor gene promoters [14–22]. This structural insight is invaluable for drug design endeavors aimed at competing with p-Tyr^{705} for binding in the SH2 cavity [21,22]. Conversely, Fig. 2b depicts the JAK2 JH1 Domain, emphasizing critical residues within the site. These include Glu^{930} and Leu^{932} of the hinge region, Leu^{855}, Gly^{856}, Lys^{857}, and Gly^{858} of the P-loop, Asp^{994} of the DFG motif, and the hydrophobic and flexible gatekeeper residue Met^{929} [41].

Finally, Fig. 2c showcases the JAK3 JH1 Domain, characterized by the typical bilobar structure of kinases, where two lobes are connected by a short linker known as the "hinge" region. This domain's primary role is to catalyze the transfer of phosphate from the ATP phosphate donor to a protein substrate [44]. The ATP binding pocket is situated between the two lobes, adjacent to the hinge, and encompasses critical residues such as Met^{902}, Glu^{903}, Tyr^{904}, Leu^{905}, Pro^{906}, and Gly^{908}. Notable features include the Glycine-rich loop (Gly^{829}, Gly^{831}, and Gly^{834}), the "Arginine pocket" (Arg^{911} and Arg^{953}), the catalytic Cys^{909}, and residues contributing to a hydrophobic environment (Val^{836} and Ala^{966}). Additionally, there's a polar triad hydrogen bond network comprising Lys^{855}, Glu^{871}, and Asp^{967}, along with Leu^{828}, Val^{884}, Ala^{853}, Asn^{954}, and Leu^{956} [45].

After analyzing the output, as detailed in Table S1 of the Supplementary Material, we selected the top 200 small molecules from each XP docking simulation. Subsequently, we focused on the common structures present in every simulation, resulting in the identification of 44 small molecules. The docking score values for each ON target are provided in Table S2 of the Supplementary Material. Moving beyond the conventional rigid receptor approximation inherent in structure-based virtual screening, we employed the Induced Fit Docking (IFD) protocol. This approach predicts the impact of ligand docking on protein structure by elucidating the structural features of ligand/target complexes and analyzing their mutual conformational changes.

In the second step of the docking workflow, IFD studies were conducted utilizing the same X-ray structure depicted in Fig. 2a–c. The output results are outlined in Table S3 of the Supplementary Material, while the IFD score for the top 20 small molecules is presented in Table 1. In this analysis we included a validation set of 9 compounds as well-known inhibitors of JAK2, JAK3, and STAT3 (***filgotinib***, ***gandotinib***, and ***ruxolitinib*** for JAK2 [46–48]; ***ritlecitinib***, ***upadacitinib***, and ***FM475*** for JAK3 [49,50]; ***BP-1-102***, ***SH5-07*** and ***SI109*** for STAT3 [51,52]).

The analysis of the Induced Fit Docking (IFD) simulations reveals that numerous compounds demonstrate effective interactions with the target proteins, yielding IFD scores that are either higher or comparable to those of the reference ligands. Notably, among the 20 structures listed in Table 1, compound **755435** consistently emerges as the most promising, achieving IFD score values of: -1188.82 for STAT3, boasting the highest score in the series; −722.75 for JAK2, exceeding other ligands including ***ruxolitinib*** (-717.95); and −656.61 for JAK3, with a notable margin compared to the co-crystalized ligand ***FM475***. Furthermore, derivative **755435** surpasses other compounds included in the validation set (***filgotinib*** and ***gandotinib*** for JAK2, ***ritlecitinib*** and ***upadacitinib*** for JAK3, ***BP-1-102*** and ***SH5-07*** for STAT3). In summary,

Table 1
IFD score of the 20 best-ranked selected small molecules, the reference co-crystalized ligands ***SI109***, ***ruxolitinib***, and ***FM475*** against STAT3 (PDB code 6NUQ), JAK2 (PDB code 6VGL), and JAK3 (PDB code 6GL9) [41–43], and the well-known inhibitors ***filgotinib*** and ***gandotinib*** for JAK2, ***ritlecitinib*** and ***upadacitinib*** for JAK3, ***BP-1-102*** and ***SH5-07*** for STAT3.

STAT3		JAK2		JAK3	
Title	IFDScore	Title	IFDScore	Title	IFDScore
SI109	−1197.26	**755435**	−722.75	684134	−658.52
755435	−1188.82	684134	−721.10	**755435**	−656.61
647610	−1187.17	707556	−719.96	647610	−655.92
707556	−1187.07	668891	−719.35	707566	−654.83
684134	−1186.62	***gandotinib***	−718.70	707556	−654.69
733269	−1186.45	647610	−718.52	697491	−654.36
697491	−1185.86	627737	−718.52	627737	−653.90
BP-1-102	−1185.61	707567	−718.59	753193	−653.88
753193	−1185.42	***filgotinib***	−717.99	732491	−653.62
707566	−1185.32	***ruxolitinib***	−717.95	668891	−653.48
SH5-07	−1184.71	732491	−717.84	707567	−653.26
707567	−1184.53	707566	−717.09	673596	−653.21
707571	−1184.53	625894	−716.95	707571	−652.95
625894	−1184.47	697491	−716.67	733269	−651.82
732491	−1183.20	707571	−716.46	625894	−651.82
668891	−1183.11	733269	−716.17	***Ritlecitinib***	−651.06
627737	−1182.33	673596	−716.12	***FM475***	−649.82
673596	−1182.15	753193	−715.83	***Upadacitinib***	−649.40

compound **755435** exhibits remarkable potential as an inhibitor for all three targets. Fig. 3a illustrates the 2D structure of compound **755435**, while Fig. 3b–d depict the 3D complexes formed between **755435** and STAT3, JAK2, and JAK3, respectively. These visual representations further underscore the compound promising interactions with the target proteins. The key interactions formed by compound **755435** with each protein binding site, were investigated and reported in Table 2.

In the JAK2 JH1 Domain, compound **755435** engaged in numerous interactions with critical residues of the active site. Notably, the hinge region played a pivotal role, akin to the co-crystallized ligand ***ruxolitinib***, involving key residues such as Glu^{930}, Tyr^{931}, Leu^{932}, Gly^{935}, Ser^{936}, and Asp^{939}. Among these, Asp^{939} formed a hydrogen bond between the oxygen atom of its side chain and the hydrogen atom of the phenolic group of compound **755435** (O—H-O). Additional hydrogen bonds were established between the N-H backbone of Phe^{860} and Gly^{861} and the amidic moiety of the compound (N-H—O), as well as between the oxygen atom of the Gly^{996} backbone and the phenolic group of the compound (O—H-O), with Pi-Pi stacking interaction involving Lys^{882}. Furthermore, hydrophobic interactions were observed with the flexible gatekeeper residue Met^{929}, the amino acids of the P-loop (Leu^{855}, Gly^{856}, Lys^{857}, and Gly^{858}), and Asp^{994} of the DFG motif. Additionally, the compound interacted with surrounding amino acids of the binding pocket, including Asn^{859}, Ser^{862}, Val^{863}, Ala^{880}, Lys^{883}, Leu^{884}, Phe^{895}, Arg^{980}, Asn^{981}, Leu^{983}, and Gly^{993}. In the JAK3 JH1 Domain, compound **755435** formed stabilizing interactions with key residues of the binding pocket, particularly in the hinge region (Met^{902}, Glu^{903}, Tyr^{904}, Leu^{905}, Pro^{906}, Gly^{908}). Multiple hydrogen bonds were formed with phenolic and amidic groups, with the hydrogen atom of the O-H group in the Tyr^{904} side chain acting as an H-bond donor. Other stabilizing H-bonds were formed near the hinge region, involving the O-H phenolic of **755435** with the N-H backbone of the catalytic Cys^{909} and the O-H group of the side chain of Asp^{912}. Furthermore, interactions with the backbone oxygen atom of Arg^{953} in the "Arginine pocket" and other crucial residues of the active site, including Gly^{829}, Gly^{831} (Glycine-rich loop), Val^{836}, Leu^{828}, Lys^{830}, Ala^{853}, Lys^{855}, Leu^{875}, Val^{884}, Arg^{916}, Asn^{954}, Leu^{956}, Ala^{966}, and Asp^{967}, were observed. Concerning the STAT3 SH2 Domain, although the number of interactions created was lower than the reference ligand, the compound **755435** fulfilled essential requirements akin to the reference ligand ***SI109***. These included the formation of hydrogen bonds between the oxygen atom of the Ser^{636} backbone and the phenolic group of the compound, the N-H backbone of

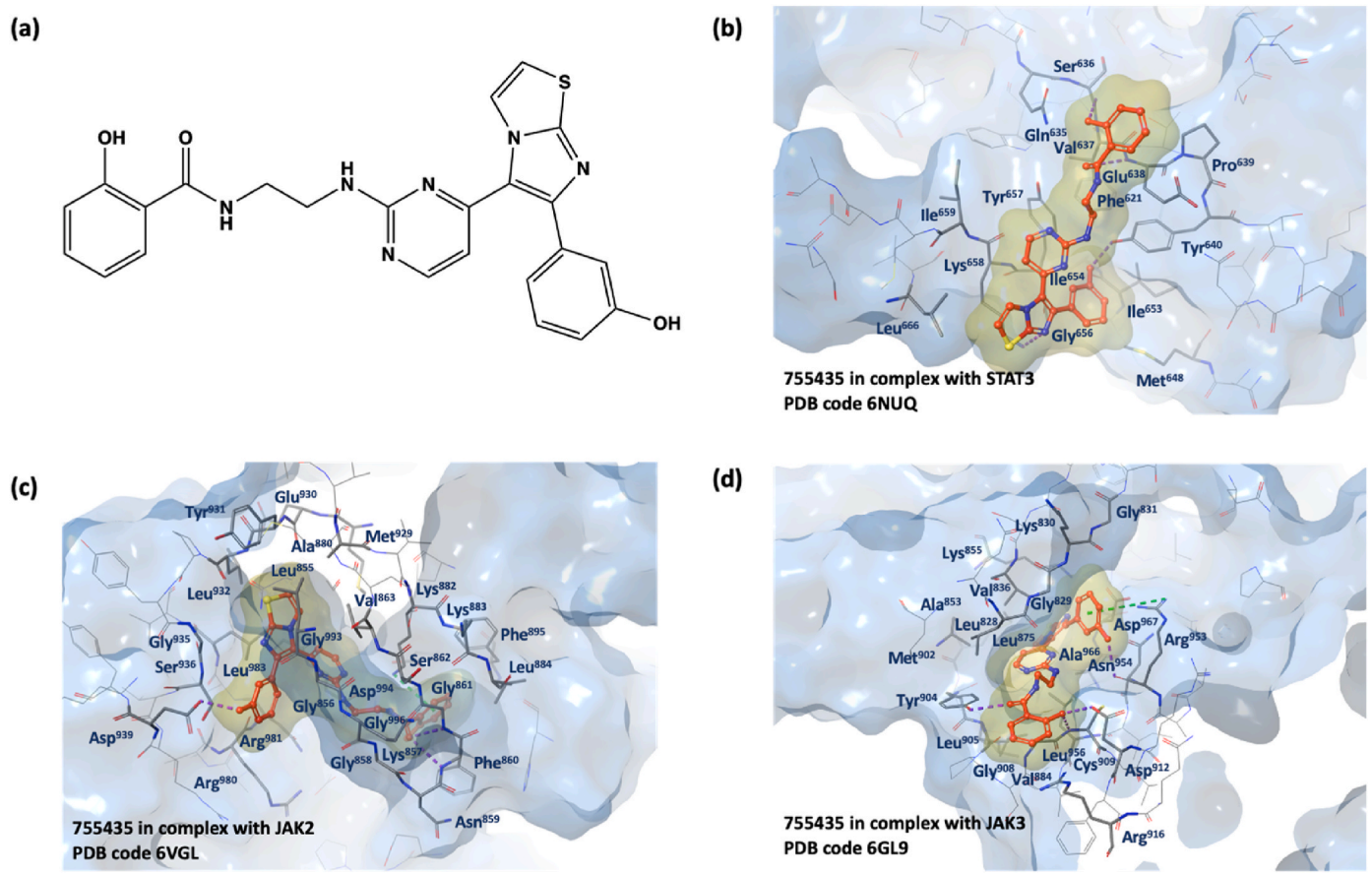

Fig. 3. a–d. (a) 2D chemical structure of compound **755435**; **(b)** STAT3 SH2 domain in complex with compound **755435**; **(c)** 3D x-ray structure of JAK2 JH1 domain in complex with compound **755435**; **(d)** 3D x-ray structure of JAK3 JH1 domain in complex with compound **755435**.

Glu^{638} and the amidic moiety of the compound, and interactions with Gln^{635}, Val^{637}, Pro^{639}, Gly^{656}, Tyr^{657}, and Lys^{658}. Additionally, a hydrophobic interaction network was observed with Phe^{621}, Met^{648}, Ile^{654}, Ile^{659}, and Leu^{666}.

2.4. Molecular dynamics simulations

Molecular Dynamics Simulations were conducted to delve into the structural characteristics of the **755435**/JAK2, **755435**/JAK3, and **755435**/STAT3 complexes. This approach allowed us to explore the dynamic behavior of molecular systems, tracking the trajectories of individual atoms and molecules as they evolve over time.

The Molecular Dynamics duration (100ns) allows for the extraction of meaningful information regarding the proteins and ligands in each complex within the same timeframe, such as Root Mean Square Deviation (RMSD), Protein Root Mean Square Fluctuation (P-RMSF), and Ligand Root Mean Square Fluctuation (L-RMSF).

The Root Mean Square Deviation (RMSD) was computed for both the ligand and protein throughout the trajectory of simulations lasting 100 ns for each ligand-protein complex. This analysis aimed to evaluate the stability and convergence of the simulations by measuring the average change in displacement of the backbone from a reference frame at t = 0. According to the RMSD analysis, depicted in Fig. 4a–c, compound **755435** demonstrated satisfactory stability within the binding sites. Specifically, the left Y-axis of the plots illustrates the evolution of RMSD for JAK2, JAK3, and STAT3, respectively, indicating the structural conformation changes during the simulations. Importantly, the RMSD values of the proteins remained within the acceptable range of 1–3 Å, signifying the maintenance of structural integrity. Meanwhile, the right Y-axis of the plots illustrates the RMSD value of **755435** throughout the simulation.

Although the RMSD of **755435** complexed to STAT3 reaches approximately 10 Å, we confirm that the ligand remained within its initial binding site throughout the simulation and did not diffuse away. Moreover, the convergence of the RMSD values of both the protein and ligand towards the end of the simulations suggests that the systems reached equilibration, reinforcing the stability of the complexes.

The Protein Root Mean Square Fluctuation (P-RMSF) analysis was conducted to examine the fluctuations of specific residues throughout the simulation in detail. Fig. 5a–c depict P-RMSF plots for each protein (JAK2, JAK3, and STAT3, respectively), where peaks indicate regions experiencing significant fluctuations. These results reveal heightened flexibility in terminal regions compared to more rigid secondary structure elements. Peaks in the P-RMSF plots pinpoint areas crucial for protein function or interactions, offering valuable insights into the dynamics of the molecular system.

Throughout the simulation, the dynamics of protein secondary structure elements (SSE), such as alpha-helices and beta-strands, for JAK2, JAK3, and STAT3 are meticulously tracked. The results of this analysis are presented in Figs. S1–S3 of the Supplementary Material.

The Ligand Root Mean Square Fluctuation (L-RMSF) serves as a crucial metric for tracking changes in the positions of ligand atoms during molecular dynamics simulations. In this study, L-RMSF analysis was conducted for compound **755435** within each complex formed by JAK2, JAK3, and STAT3. The reference time (tref) was set to the first frame, establishing it as the zero point in time. The L-RMSFs, illustrated in Fig. 6b–d for JAK2, JAK3, and STAT3 complexes respectively, offer a detailed breakdown of ligand atomic-level fluctuations. These fluctuations are visually represented in Fig. 6a as a 2D structure. This information provides insights into how specific ligand fragments interact

Table 2
Overview of the amino acids involved in the binding of the selected compound **755435** in the binding sites of STAT3, JAK2, and JAK3, compared to co-crystalized ligands ***SI109***, ***ruxolitinib***, and ***FM475***, at 4 Å proximity.

STAT3 SH2 Domain			JAK2 JH1 Domain			JAK3 JH1 Domain		
Title	*Sl109*	755435	Title	*ruxolitinib*	755435	Title	*FM475*	755435
Lys^{591}	X[a]		Leu^{855}	X	X	Leu^{828}	X[a]	X
Arg^{609}	X[a]		Gly^{856}	X	X	Gly^{829}	X	X
Ser^{611}	X[a]		Lys^{857}	X	X	Lys^{830}		X
Glu^{612}	X[a]		Gly^{858}	X	X	Gly^{831}		X
Ser^{613}	X		Asn^{859}		X	Val^{836}	X	X
Ser^{614}	X		Phe^{860}		[a]X	Ala^{853}	X	X
Thr^{620}	X		Gly^{861}	X	[a]X	Lys^{855}	X	X
Phe^{621}		X	Ser^{862}	X	X	Glu^{871}	X	
Trp^{623}	X		Val^{863}	X	X	Leu^{875}		X
Gln^{635}	X	X	Ala^{880}	X	X	Val^{884}	X	X
Ser^{636}	X[a]	X[a]	Lys^{882}	X	[#]X	Met^{902}	X	X
Val^{637}	X	X	Lys^{883}		X	Glu^{903}	X	
Glu^{638}	X[a]	X[a]	Leu^{884}		X	Tyr^{904}	X	[a]X
Pro^{639}	X[a]	X	Phe^{895}		X	Leu^{905}	X	X
Tyr^{640}	X	X[a]	Val^{911}	X		Pro^{906}	X	
Thr^{641}	X		Met^{929}	X	X	Gly^{908}	X	X
Gln^{644}	X[a]		Glu^{930}	[a]X	X	Cys^{909}	X	[a]X
Met^{648}		X	Tyr^{931}	X	X	Asp^{912}		[a]X
Ile^{653}		X[a]	Leu^{932}	[a]X	X	Arg^{916}		X
Ile^{654}		X	Gly^{935}		X	Arg^{953}	X	[a]X
Gly^{656}	X	X	Ser^{936}		X	Asn^{954}	X	X
Tyr^{657}	X[a]	X	Asp^{939}		[a]X	Leu^{956}	X	X
Lys^{658}	X	X	Arg^{980}	X	X	Ala^{966}	X	X
Ile^{659}		X	Asn^{981}	X	X	Asp^{967}	X	X
Leu^{666}		X	Leu^{983}	X	X			
			Gly^{993}	X	X			
			Asp^{994}	X	X			
			Gly^{996}		[a]X			
Tot.	**19**	**15**	**Tot**	**19**	**27**	**Tot.**	**19**	**21**

The derivative **755435** exhibited a comparable number of interactions to the co-crystallized ligands ***SI109***, ***ruxolitinib***, and ***FM475***, within a 4 Å proximity.
[a] H-bonds.

with the protein and contribute to the entropic aspects of the binding event. The 'Fit Ligand on Protein' line depicted in the figures illustrates ligand fluctuations relative to the protein environment. By aligning the protein-ligand complex on the protein backbone and measuring the L-RMSF on its heavy atoms, this line demonstrates how the ligand dynamically responds within the context of the protein environment.

In summary, compound **755435** demonstrates stability, with an overall RMSF ranging from 1 to 8 Å. This stability is particularly noteworthy as it indicates a consistent and well-defined binding mode throughout the simulations. Additionally, the ligand torsion profile, summarizing the conformational evolution of every rotatable bond in compound **755435**, was accurately analyzed throughout the simulation. The results of this analysis are presented in Fig. S4 of the Supplementary Material.

Subsequently, a range of structural parameters was computed for each complex to offer a comprehensive analysis of their molecular features. This included the calculation of the Radius of Gyration (rGyr), which assesses the "extendedness" of the ligand and correlates with its principal moment of inertia. Additionally, parameters such as Intramolecular Hydrogen Bonds (intraHB), Molecular Surface Area (MolSA), Solvent Accessible Surface Area (SASA), and Polar Surface Area (PSA) were determined. The findings from these calculations are presented and discussed in the Supplementary Material (Figs. S5–S7).

Molecular Dynamics Simulations for reference compounds within the validation set, in complex with respective proteins, have been conducted. RMSD, P-RMSF, L-RMSF, SSE analysis have been reported in the Supplementary Material as Figs. S8–S15. Finally, we analyzed the conformational space and energies of complexes across Molecular Dynamics Simulations studies. Fig. S16 (Supplementary Material) depicts plots of protein–ligand contacts and explains the interaction fraction of the protein residue with the ligand, which explains how much (%) of the simulation time of the specific interaction is maintained between ligand and receptors complexes. Table S3 (Supplementary Material) shows a summary of performed MM-GBSA analysis, describing Coulomb, van der Waals and solvent energies for **755435**/JAK2, **755435**/JAK3, **755435**/STAT3, ***ruxolitinib***/JAK2, ***filgotinib***/JAK2, ***gandotinib***/JAK2, ***retlicitinib***/JAK3, ***upadacitinib***/JAK3, ***FM745***/JAK3, ***BP-1-102***/STAT3, ***SH5-07***/STAT3, and ***SI109***/STAT3 complexes. Furthermore, output data from Molecular Dynamics Simulation are available in Supplementary Material 3.

3. Material and methods

3.1. Database cleaning phase

In this study, we utilized two widely recognized computational tools, QikProp and SwissADME, to evaluate the pharmacokinetic profiles of the designed compounds and to identify those lacking drug-like properties. QikProp [31], an integral part of the Schrödinger Suite, employs molecular descriptors to predict various drug-like attributes, such as solubility, permeability, and bioavailability. Default settings were employed for calculations, yielding insights into the compounds' ADME (Absorption, Distribution, Metabolism, and Excretion) properties. Moreover, we employed SwissADME, an online platform developed by the Swiss Institute of Bioinformatics, to further assess the pharmacokinetic parameters. SwissADME utilizes robust algorithms to estimate physicochemical properties, drug-likeness, and medicinal chemistry-related parameters. The integration of QikProp and SwissADME analyses provided a comprehensive understanding of the potential drug-like characteristics of the investigated compounds, facilitating the selection of lead candidates for subsequent experimental validation.

3.2. Ligand-based studies

The web service DRUDIT (www.drudit.com, accessed on April 08,

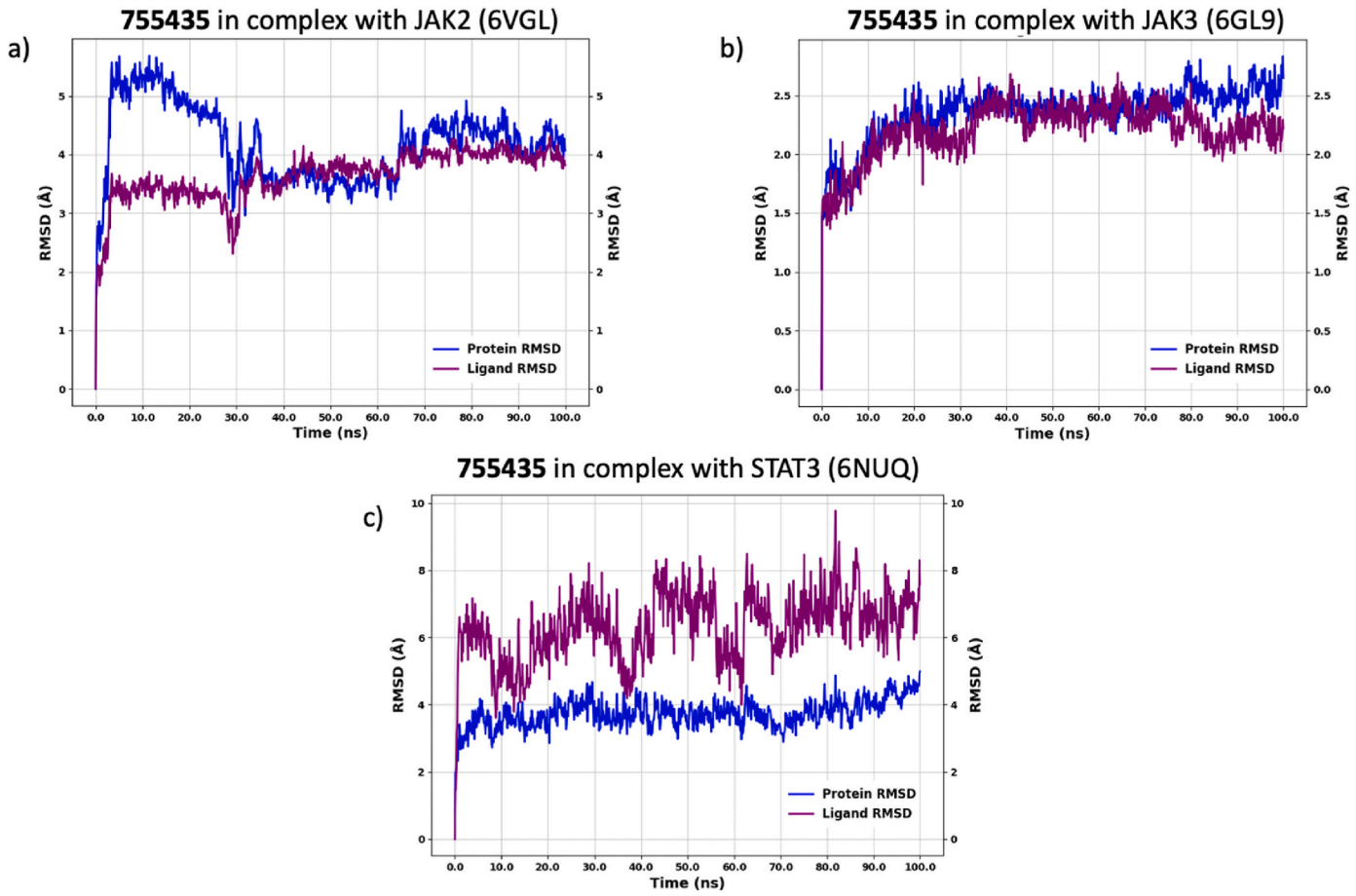

Fig. 4. **(a)** Calculated RMSD during the simulation trajectory of 100ns for **755435**/JAK2 complex; **(b)** calculated RMSD during the simulation trajectory of 100ns for **755435**/JAK3 complex; **(c)** calculated RMSD during the simulation trajectory of 100ns for **755435**/STAT3 complex.

2024) operates on four servers, each capable of concurrently handling more than ten jobs. These servers run various software modules implemented in C and JAVA on MacOS Mojave. Specifically, the Biotarget Finder Module was employed in a combined ON/OFF-targets/Multitarget Mode to screen the extensive, meticulously cleaned NCI database of active small molecules for potential JAK/STAT inhibitors, while ensuring minimal impact on the OFF targets TNF-α and p53 [33].

The Biotarget Predictor Tool (BPT) facilitates the prediction of binding affinity between candidate molecules and specified biological targets. Templates of ON and OFF targets (STAT3, JAK2, JAK3, TNF-α, and p53) were constructed using sets of well-established protein inhibitors with affinities <100 nM, sourced from BindingDB [34]. Molecular docking studies were then conducted at each respective binding site to securely position ligands within the pockets. Molecular descriptors were computed using MOLDESTO. Five molecular descriptor target templates were integrated into DRUDIT, employing default parameters (N = 500, Z = 50, G = a) [33,40].

In the initial phase of the *in silico* workflow, the meticulously curated NCI database was uploaded to DRUDIT and subjected to the Biotarget Predictor in a combined ON/OFF-targets/Multitarget Mode. The output results yielded a Drudit Affinity Score (DAS) value for each structure, representing the binding affinity of compounds against the ON targets JAK2, JAK3, and STAT3, as well as the OFF targets TNF-α and p53.

In detail, DAS χ and DAS γ were first calculated by equations (2) and (3) as follows:

$$DAS\chi = \mathrm{DAS}_{STAT3} \times \mathrm{DAS}_{JAK2} \times \mathrm{DAS}_{JAK3} \tag{2}$$

$$DAS\gamma = \mathrm{DAS}_{TNF\alpha} \times \mathrm{DAS}_{p53} \tag{3}$$

Finally, the "Multi-ON/OFF Target Score" was computed with equation (1):

$$\mathrm{Multi} - \frac{\mathrm{ON}}{\mathrm{OFF}}\mathrm{Target\ Score} = \frac{DAS\chi}{DAS\gamma} \tag{1b}$$

3.3. Strucuture-based studies

The preparation of ligands and proteins for *in silico* studies adhered to the following meticulously detailed procedures.

3.3.1. Ligand preparation

The ligands earmarked for docking were prepared using the LigPrep tool within the Schrödinger Maestro Suite [53]. Each ligand underwent exhaustive tautomer and stereoisomer generation at a pH of 7.0 ± 0.4, employing default settings and the Epik ionization method [54]. Following this, the Optimized Potentials for Liquid Simulations (OPLS 2005) force field was employed to minimize the energy status of the ligands [55].

3.3.2. Protein Preparation

Crystal structures of JAK2, JAK3, and STAT3 (PDB codes 6VGL [41], 6GL9 [43], and 6NUQ [42], respectively) were retrieved from the Protein Data Bank [56,57]. Using the Protein Preparation Wizard within the Schrödinger software suite, default settings were applied to prepare these structures [58]. This involved assigning bond orders, including the Het group, eliminating all water molecules, and adjusting heteroatom states using the Epik tool, with the pH set to biologically relevant values (7.0 ± 0.4). Subsequently, optimization of the H-bond network was

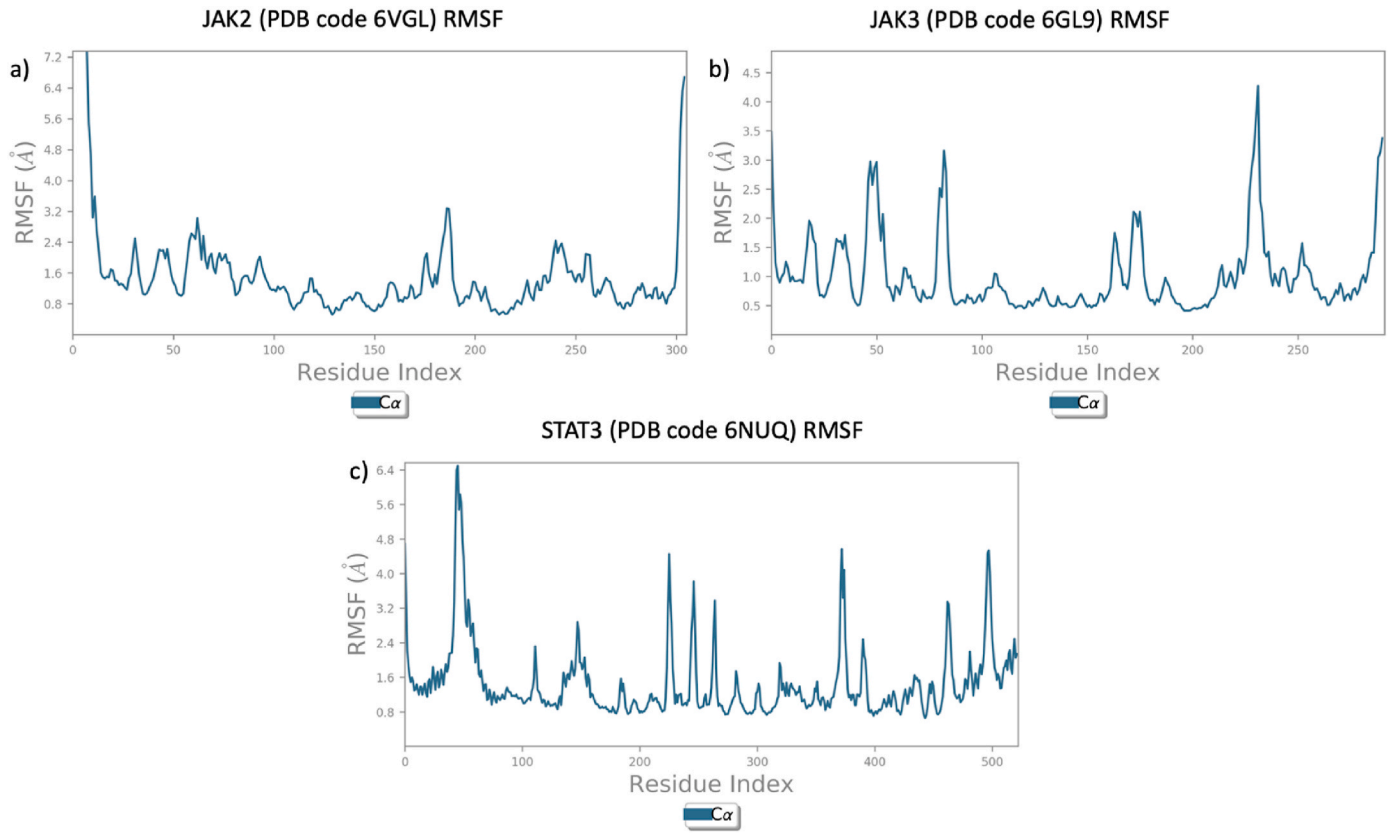

Fig. 5. **(a)** Calculated P-RMSF during the simulation for JAK2; **(b)** calculated P-RMSF during the simulation for JAK3; **(c)** calculated P-RMSF during the simulation for STAT3.

conducted, followed by a restrained energy minimization step (with an RMSD of atom displacement set at 0.3 Å), utilizing the OPLS 2005 force field [55].

3.3.3. Docking validation

The molecular docking investigations were conducted using the Glide module within the Schrödinger Suite. Receptor grids were generated by designating the original ligands ***ruxolitinib*** (for JAK2, PDB code 6VGL [41]), ***FM475*** (for JAK3, PDB code 6GL9 [43]), and ***SI109*** (for STAT3, PDB code 6NUQ [42]) as the centroids of the grid boxes. This led to set the enclosing box size as a cube with sides of length 26 Å, and point separation of 2.89 Å. The residue-atom notation nearest to the center of the docking grid for each crystallographic structure is as follows: for JAK2, the residue is Val^{863} with an H-CH_2 atom ($Val^{863}CH_3$); for JAK3, the residue is Leu^{956} with an H-CH_2 atom ($Leu^{956}CH_3$); and for STAT3, the residue is Glu^{638} with an H-N atom ($Glu^{638}NH$). Employing the Extra Precision (XP) mode as the scoring function, 3D conformers were docked into the receptor model. A post-docking minimization step was executed for each ligand conformer, generating a maximum of 2 docking poses and a total of 5 poses per ligand conformer. Notably, the docking protocol successfully redocked the original ligands within the receptor-binding pockets with an RMSD < 0.51 Å.

The Extra Precision (XP) Docking was employed to preliminarily screen compounds selected by DRUDIT. The Induced Fit Docking (IFD) simulation was conducted using the Schrödinger IFD application, a precise and robust technology accommodating both ligand and receptor flexibility [59,60]. Applying Schrödinger's validated IFD protocol, JAK2, JAK3, and STAT3 proteins (PDB codes 6VGL [41], 6GL9 [43], and 6NUQ [42], respectively), previously refined by the Protein Preparation module, were used. The IFD score, calculated as IFD score $= 1.0$ Glide Gscore $+0.05$ Prime Energy, incorporating protein-ligand interaction energy and system total energy, was utilized to rank the IFD poses.

3.3.4. Molecular dynamics simulation

To assess the stability and binding affinity of the **755435**/JAK2, **755435**/JAK3, and **755435**/STAT3 complexes, Molecular Dynamics Simulations were conducted using the Desmond software. The simulations were performed under the constant-temperature–constant-pressure ensemble (NPT), allowing precise control over both temperature and pressure conditions. Pressure adjustments within the NPT ensemble were achieved by modifying the volume, while the unit cell vectors were allowed to change. Simulation parameters were configured with a system temperature of 300 K and a pressure of 1013.25 bar. The Nose-Hoover Chain thermostat and the Martyna-Tobias-Klein barostat were settled with a relaxation time of 1ps, and 2ps, respectively. Before commencing the production run, the systems underwent energy minimization for 1000 steps to establish a stable starting point. Subsequently, a production run of 100ns was conducted for the **755435**/JAK2, **755435**/JAK3, and **755435**/STAT3 complexes, respectively. The simulation results were meticulously analyzed to observe the time-lapse binding energy for both the protein and ligand, Root Mean Square Deviation (RMSD), Root Mean Square Fluctuation (RMSF), and Radius of Gyration (rGyr). This comprehensive analysis offers crucial insights into the dynamic behavior of the complexes, providing valuable information about their structural integrity and the nature of molecular interactions over the simulation period.

4. Conclusions

Apoptosis plays a pivotal role in maintaining cellular health and regulating immune responses by eliminating damaged or unnecessary cells within the body. Dysregulation of JAK/STAT signaling, crucial in the life-and-death balance of human cells, is implicated in various cancers and diseases, making it a promising therapeutic target.

In this study, we employed an innovative computational approach to

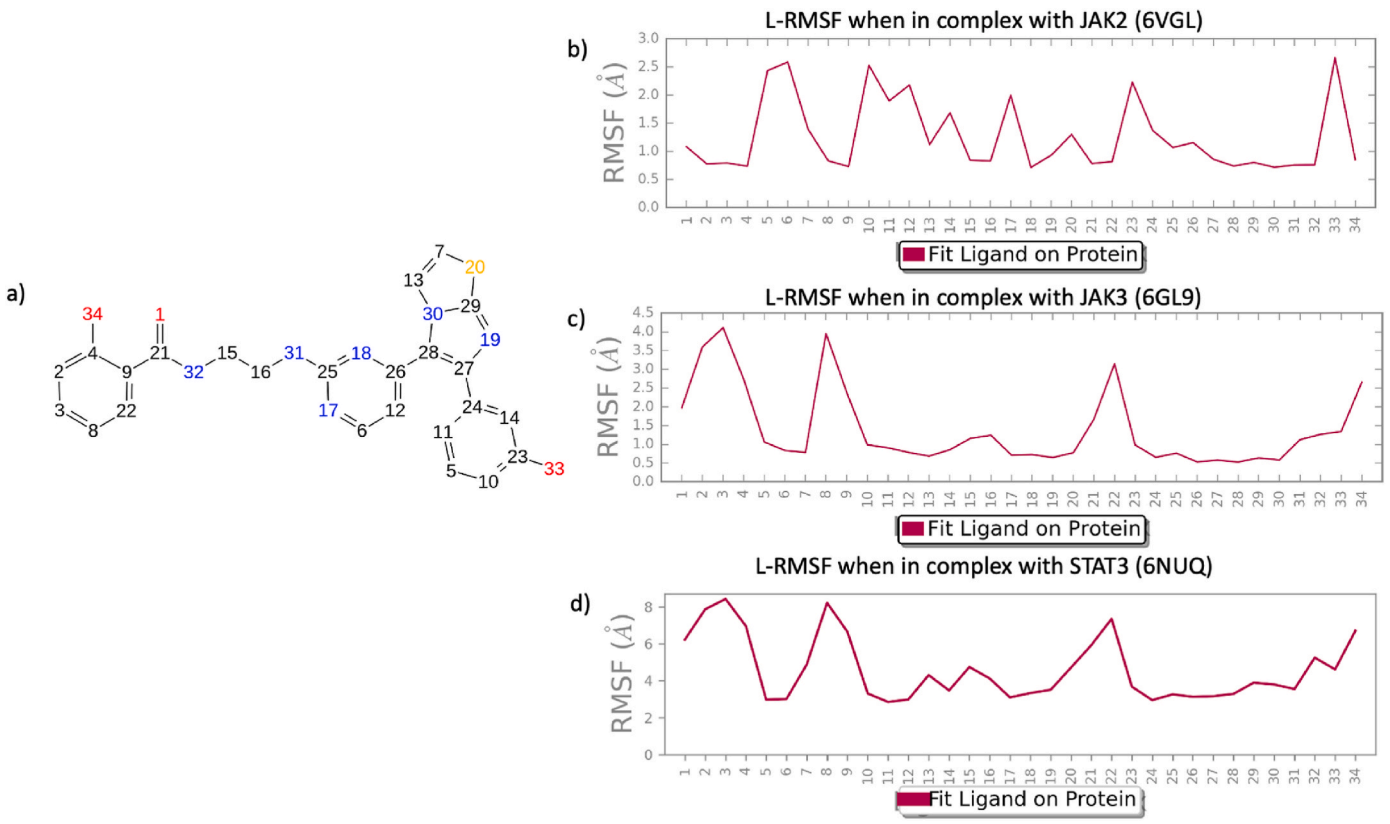

Fig. 6. **(a)** 2D structure of compound **755435**; **(b)** calculated L-RMSF during the simulation for **75543** when in complex with JAK2; (c) calculated L-RMSF during the simulation for **755435** when in complex with JAK3; **(d)** calculated L-RMSF during the simulation for **755435** when in complex with STAT3.

identify potential inhibitors capable of targeting key proteins involved in apoptotic pathways, with a specific focus on JAK2, JAK3, and STAT3, while minimizing affinity for OFF-targets such as TNF-α and p53. Our methodology involved a meticulous cleaning phase of the NCI database using QikProp and SwissADME tools. The cleaned database underwent ligand-based studies using the Biotarget Predictor Tool (BPT) in a combined ON/OFF-targets/Multitarget mode. Subsequent Molecular Docking investigations led to the identification of compound **755435**, exhibiting binding affinities for JAK2, JAK3, and STAT3 comparable to reference ligands, suggesting its potential as a viable therapeutic agent. Furthermore, Molecular Dynamics Simulations established the potential compound ability to interact with the target binding sites, indicating a potential multi-target inhibition mode of action. The prospect of a unique molecule with multi-target activity could reduce the need for mixed therapy, enhancing patient compliance, minimizing the risk of adverse drug interactions, and facilitating the identification of desired therapeutic effects and possible adverse reactions. In light of these findings, we propose an *in silico* mixed ligand/structure-based protocol for designing JAK/STAT multi-target inhibitors, with low affinity for the OFF-targets TNF-α and p53, as potential anticancer agents for the treatment of various tumoral diseases.

Supplementary Materials: The following supporting information can be downloaded at: www.mdpi.com/xxx/s1, Matrix S1: DA

S values of structures for each target (ON/OFF targets); Matrix S2: top-ranked 5 % of molecules; Table S1: top 200 small molecules from each XP docking simulation; Table S2: docking score values for each ON target for the identified small molecules; Table S3: IFD score for the identified common structures; Figs. S1–S3: Summary of the tracked protein Secondary Structure Elements (SSE) for JAK2 (S1), JAK3 (S2), and STAT3 (S3); Fig. S4: 2D schematic representation of compound **755435** and rotatable bond torsion dial plot; Figs. S5–S7: Detailed outcomes results for complexes **755435**/JAK2 (S5), **755435**/JAK3 (S6), and **755435**/STAT3 (S7); Fig. S8: Calculated RMSD during the simulation trajectory of 100ns for ***ruxolitinib***/JAK2, ***FM745***/JAK3, and ***SI109***/STAT3; Fig. S9: Calculated P-RMSF during the simulation for JAK2, JAK3, and STAT3; Fig. S10: 2D structure of ***ruxolitinib***, ***FM475***, and ***SI109***, and calculated L-RMSF during the simulation for ***ruxolitinib*** in complex with JAK2, ***FM475*** in complex with JAK3, and ***SI109*** in complex with STAT3; Figs. S11–S13: Summary of the tracked protein Secondary Structure Elements (SSE) for JAK2 (S11), JAK3 (S12), and STAT3 (S13); Fig. S14: Protein–ligand interactions examination across the simulation time for **755435**/JAK2, **755435**/JAK3, **755435**/STAT3, ***ruxolitinib***/JAK2, ***FM475***/JAK3, and ***SI109***/JAK2; Table S4: Summary of MM-GBSA analysis. Supplementary Material 3: Molecular Dynamics Simulation Output files.

CRediT authorship contribution statement

Alessia Bono: Writing – original draft, Visualization, Validation, Methodology, Investigation, Formal analysis, Data curation, Conceptualization. **Gabriele La Monica:** Writing – original draft, Visualization, Validation, Formal analysis. **Federica Alamia:** Writing – original draft, Visualization, Validation. **Antonino Lauria:** Writing – original draft, Supervision, Software, Resources, Project administration, Methodology, Investigation, Funding acquisition, Data curation, Conceptualization. **Annamaria Martorana:** Writing – original draft, Visualization, Methodology, Formal analysis, Data curation.

Informed consent statement

Not applicable.

Institutional review board statement

Not applicable.

Funding

This research was funded by SiciliAn MicronanOTecH Research and Innovation CEnter "SAMOTHRACE" (MUR, PNRR-M4C2, ECS_00000022), spoke 3-Università degli Studi di Palermo "S2-COMMs-Micro and Nanotechnologies for Smart & Sustainable Communities.

Declaration of competing interest

The authors declare that they have no known competing financial interests or personal relationships that could have appeared to influence the work reported in this paper.

Acknowledgments

The authors would like to thank also the "National Biodiversity Future Center"(identification code CN00000033, CUP B73C22000790001) on 'Biodiversity', financed under the National Recovery and Resilience Plan (NRRP), Mission 4, Component 2, Investment 1.4 "Strengthening of research structures and creation of R&D 'national champions' on some Key Enabling Technologies"—Call for tender No. 3138 of December 16, 2021, rectified by Decree n.3175 of December 18, 2021 of Italian Ministry of University and Research funded by the European Union—NextGenerationEU.

Appendix A. Supplementary data

Supplementary data to this article can be found online at https://doi.org/10.1016/j.jmgm.2024.108913.

Data availability

Data will be made available on request.

References

[1] X. Xu, Y. Lai, Z.C. Hua, Apoptosis and apoptotic body: disease message and therapeutic target potentials, Biosci. Rep. 39 (2019), https://doi.org/10.1042/BSR20180992.
[2] M.S. D'Arcy, Cell death: a review of the major forms of apoptosis, necrosis and autophagy, Cell Biol. Int. 43 (2019) 582–592, https://doi.org/10.1002/cbin.11137.
[3] D. Kashyap, V.K. Garg, N. Goel, Intrinsic and extrinsic pathways of apoptosis: role in cancer development and prognosis, Adv. Protein Chem. Struct. Biol. 125 (2021) 73–120, https://doi.org/10.1016/bs.apcsb.2021.01.003.
[4] P. Xin, X. Xu, C. Deng, S. Liu, Y. Wang, X. Zhou, H. Ma, D. Wei, S. Sun, The role of JAK/STAT signaling pathway and its inhibitors in diseases, Int. Immunopharm. 80 (2020) 106210, https://doi.org/10.1016/j.intimp.2020.106210.
[5] X. Hu, J. Li, M. Fu, X. Zhao, W. Wang, The JAK/STAT signaling pathway: from bench to clinic, Signal Transduct. Targeted Ther. 6 (2021) 402, https://doi.org/10.1038/s41392-021-00791-1.
[6] N.C. Reich, STATs get their move on, JAK-STAT 2 (2013) e27080, https://doi.org/10.4161/jkst.27080.
[7] G. La Sala, C. Michiels, T. Kükenshöner, T. Brandstoetter, B. Maurer, A. Koide, K. Lau, F. Pojer, S. Koide, V. Sexl, et al., Selective inhibition of STAT3 signaling using monobodies targeting the coiled-coil and N-terminal domains, Nat. Commun. 11 (2020) 4115, https://doi.org/10.1038/s41467-020-17920-z.
[8] B. Rah, R.A. Rather, G.R. Bhat, A.B. Baba, I. Mushtaq, M. Farooq, T. Yousuf, S. B. Dar, S. Parveen, R. Hassan, et al., JAK/STAT signaling: molecular targets, therapeutic opportunities, and limitations of targeted inhibitions in solid malignancies, Front. Pharmacol. 13 (2022) 821344, https://doi.org/10.3389/fphar.2022.821344.
[9] A. Ou, M. Ott, D. Fang, A.B. Heimberger, The role and therapeutic targeting of JAK/STAT signaling in glioblastoma, Cancers 13 (2021), https://doi.org/10.3390/cancers13030437.
[10] X. Yang, Z. Tang, P. Zhang, L. Zhang, Research advances of JAK/STAT signaling pathway in lung cancer], Zhongguo Fei Ai Za Zhi 22 (2019) 45–51, https://doi.org/10.3779/j.issn.1009-3419.2019.01.09.
[11] O. Silvennoinen, D. Ungureanu, Y. Niranjan, H. Hammaren, R. Bandaranayake, S. R. Hubbard, New insights into the structure and function of the pseudokinase domain in JAK2, Biochem. Soc. Trans. 41 (2013) 1002–1007, https://doi.org/10.1042/BST20130005.
[12] C. Xue, Q. Yao, X. Gu, Q. Shi, X. Yuan, Q. Chu, Z. Bao, J. Lu, L. Li, Evolving cognition of the JAK-STAT signaling pathway: autoimmune disorders and cancer, Signal Transduct. Targeted Ther. 8 (2023) 204, https://doi.org/10.1038/s41392-023-01468-7.
[13] K. Gnanasambandan, P.P. Sayeski, A structure-function perspective of Jak2 mutations and implications for alternate drug design strategies: the road not taken, Curr. Med. Chem. 18 (2011) 4659–4673, https://doi.org/10.2174/092986711797379267.
[14] C.Y. Loh, A. Arya, A.F. Naema, W.F. Wong, G. Sethi, C.Y. Looi, Signal transducer and activator of transcription (STATs) proteins in cancer and inflammation: functions and therapeutic implication, Front. Oncol. 9 (2019) 48, https://doi.org/10.3389/fonc.2019.00048.
[15] E.B. Haura, J. Turkson, R. Jove, Mechanisms of disease: insights into the emerging role of signal transducers and activators of transcription in cancer, Nat. Clin. Pract. Oncol. 2 (2005) 315–324, https://doi.org/10.1038/ncponc0195.
[16] D.E. Johnson, R.A. O'Keefe, J.R. Grandis, Targeting the IL-6/JAK/STAT3 signalling axis in cancer, Nat. Rev. Clin. Oncol. 15 (2018) 234–248, https://doi.org/10.1038/nrclinonc.2018.8.
[17] J. Bollrath, T.J. Phesse, V.A. von Burstin, T. Putoczki, M. Bennecke, T. Bateman, T. Nebelsiek, T. Lundgren-May, O. Canli, S. Schwitalla, et al., gp130-mediated Stat3 activation in enterocytes regulates cell survival and cell-cycle progression during colitis-associated tumorigenesis, Cancer Cell 15 (2009) 91–102, https://doi.org/10.1016/j.ccr.2009.01.002.
[18] H. Yu, H. Lee, A. Herrmann, R. Buettner, R. Jove, Revisiting STAT3 signalling in cancer: new and unexpected biological functions, Nat. Rev. Cancer 14 (2014) 736–746, https://doi.org/10.1038/nrc3818.
[19] Z. Wang, C. Hui, Y. Xie, Natural STAT3 inhibitors: a mini perspective, Bioorg. Chem. 115 (2021) 105169, https://doi.org/10.1016/j.bioorg.2021.105169.
[20] S. Becker, B. Groner, C.W. Müller, Three-dimensional structure of the Stat3beta homodimer bound to DNA, Nature 394 (1998) 145–151, https://doi.org/10.1038/28101.
[21] C.P. Lim, X. Cao, Structure, function, and regulation of STAT proteins, Mol. Biosyst. 2 (2006) 536–550, https://doi.org/10.1039/b606246f.
[22] S.P. Gao, J.F. Bromberg, Touched and moved by STAT3, Sci. STKE 2006 (2006) pe30, https://doi.org/10.1126/stke.3432006pe30.
[23] R.J. Shah, S. Banerjee, S. Raychaudhuri, S.P. Raychaudhuri, JAK-STAT inhibitors in Immune mediated diseases: an Overview, Indian J. Dermatol. Venereol. Leprol. 89 (2023) 691–699, https://doi.org/10.25259/IJDVL_1152_2022.
[24] S. Alvarez, A. Blanco, M. Fresno, M. Muñoz-Fernández, TNF-α contributes to caspase-3 independent apoptosis in neuroblastoma cells: role of NFAT, PLoS One 6 (2011) e16100, https://doi.org/10.1371/journal.pone.0016100.
[25] H. Wajant, K. Pfizenmaier, P. Scheurich, Tumor necrosis factor signaling, Cell Death Differ. 10 (2003) 45–65, https://doi.org/10.1038/sj.cdd.4401189.
[26] K.H. Vousden, D.P. Lane, p53 in health and disease, Nat. Rev. Mol. Cell Biol. 8 (2007) 275–283, https://doi.org/10.1038/nrm2147.
[27] A.V. Vaseva, U.M. Moll, The mitochondrial p53 pathway, Biochim. Biophys. Acta 1787 (2009) 414–420, https://doi.org/10.1016/j.bbabio.2008.10.005.
[28] X. Shao, X. Yang, J. Shen, S. Chen, X. Jiang, Q. Wang, Q. Di, TNF-α-induced p53 activation induces apoptosis in neurological injury, J. Cell Mol. Med. 24 (2020) 6796–6803, https://doi.org/10.1111/jcmm.15333.
[29] S.W. Fesik, Promoting apoptosis as a strategy for cancer drug discovery, Nat. Rev. Cancer 5 (2005) 876–885, https://doi.org/10.1038/nrc1736.
[30] Schrödinger Release 2023-3: QikProp, Schrödinger, LLC, New York, NY, 2023.
[31] A. Daina, O. Michielin, V. Zoete, SwissADME: a free web tool to evaluate pharmacokinetics, drug-likeness and medicinal chemistry friendliness of small molecules, Sci. Rep. 7 (2017) 42717, https://doi.org/10.1038/srep42717.
[32] A. Lauria, S. Mannino, C. Gentile, G. Mannino, A. Martorana, D. Peri, DRUDIT: web-based DRUgs DIscovery Tools to design small molecules as modulators of biological targets, Bioinformatics 36 (2020) 1562–1569, https://doi.org/10.1093/bioinformatics/btz783.
[33] A. Bono, A. Lauria, G. La Monica, F. Alamia, F. Mingoia, A. Martorana, In silico design of new dual inhibitors of SARS-CoV-2 MPRO through ligand- and structure-based methods, Int. J. Mol. Sci. 24 (2023) 8377.
[34] A. Bono, G. La Monica, F. Alamia, F. Mingoia, C. Gentile, D. Peri, A. Lauria, A. Martorana, In silico mixed ligand/structure-based design of new CDK-1/PARP-1 dual inhibitors as anti-breast cancer agents, Int. J. Mol. Sci. 24 (2023), https://doi.org/10.3390/ijms241813769.
[35] G. La Monica, A. Lauria, A. Bono, A. Martorana, Off-target-based design of selective HIV-1 PROTEASE inhibitors, Int. J. Mol. Sci. 22 (2021), https://doi.org/10.3390/ijms22116070.
[36] A. Lauria, A. Martorana, G. La Monica, S. Mannino, G. Mannino, D. Peri, C. Gentile, In silico identification of small molecules as new Cdc25 inhibitors through the correlation between chemosensitivity and protein expression pattern, Int. J. Mol. Sci. 22 (2021), https://doi.org/10.3390/ijms22073714.
[37] F. Mingoia, C. Di Sano, C. D'Anna, M. Fazzari, L. Minafra, A. Bono, G. La Monica, A. Martorana, A.M. Almerico, A. Lauria, Synthesis of new antiproliferative 1,3,4-substituted-pyrrolo[3,2-c]quinoline derivatives, biological and in silico insights, Eur. J. Med. Chem. 258 (2023) 115537, https://doi.org/10.1016/j.ejmech.2023.115537.
[38] G. La Monica, G. Pizzolanti, C. Baiamonte, A. Bono, F. Alamia, F. Mingoia, A. Lauria, A. Martorana, Design and synthesis of novel thieno[3,2-c] quinoline compounds with antiproliferative activity on RET-dependent medullary thyroid cancer cells, ACS Omega 8 (38) (2023) 34640–34649, https://doi.org/10.1021/acsomega.3c03578.

[39] A. Martorana, C. Gentile, A. Lauria, In silico insights into the SARS CoV-2 main Protease suggest NADH endogenous defences in the control of the pandemic coronavirus infection, Viruses 12 (2020), https://doi.org/10.3390/v12080805.
[40] T. Liu, Y. Lin, X. Wen, R.N. Jorissen, M.K. Gilson, BindingDB: a web-accessible database of experimentally determined protein-ligand binding affinities, Nucleic Acids Res. 35 (2007) D198–D201, https://doi.org/10.1093/nar/gkl999.
[41] R.R. Davis, B. Li, S.Y. Yun, A. Chan, P. Nareddy, S. Gunawan, M. Ayaz, H. R. Lawrence, G.W. Reuther, N.J. Lawrence, et al., Structural insights into JAK2 inhibition by ruxolitinib, fedratinib, and derivatives thereof, J. Med. Chem. 64 (2021) 2228–2241, https://doi.org/10.1021/acs.jmedchem.0c01952.
[42] L. Bai, H. Zhou, R. Xu, Y. Zhao, K. Chinnaswamy, D. McEachern, J. Chen, C. Y. Yang, Z. Liu, M. Wang, et al., A potent and selective small-molecule degrader of STAT3 achieves complete tumor regression in vivo, Cancer Cell 36 (2019) 498–511, https://doi.org/10.1016/j.ccell.2019.10.002, e417.
[43] M. Forster, A. Chaikuad, T. Dimitrov, E. Döring, J. Holstein, B.T. Berger, M. Gehringer, K. Ghoreschi, S. Müller, S. Knapp, et al., Development, optimization, and structure-activity relationships of covalent-reversible JAK3 inhibitors based on a tricyclic imidazo[5,4- d]pyrrolo[2,3- b]pyridine scaffold, J. Med. Chem. 61 (2018) 5350–5366, https://doi.org/10.1021/acs.jmedchem.8b00571.
[44] M.G. Cornejo, T.J. Boggon, T. Mercher, JAK3: a two-faced player in hematological disorders, Int. J. Biochem. Cell Biol. 41 (2009) 2376–2379, https://doi.org/10.1016/j.biocel.2009.09.004.
[45] J.E. Chrencik, A. Patny, I.K. Leung, B. Korniski, T.L. Emmons, T. Hall, R. A. Weinberg, J.A. Gormley, J.M. Williams, J.E. Day, et al., Structural and thermodynamic characterization of the TYK2 and JAK3 kinase domains in complex with CP-690550 and CMP-6, J. Mol. Biol. 400 (2010) 413–433, https://doi.org/10.1016/j.jmb.2010.05.020.
[46] P.G. Traves, B. Murray, F. Campigotto, R. Galien, A. Meng, J.A. Di Paolo, JAK selectivity and the implications for clinical inhibition of pharmacodynamic cytokine signalling by filgotinib, upadacitinib, tofacitinib and baricitinib, Ann. Rheum. Dis. 80 (2021) 865–875, https://doi.org/10.1136/annrheumdis-2020-219012.
[47] A. Rosenthal, R.A. Mesa, Janus kinase inhibitors for the treatment of myeloproliferative neoplasms, Expet Opin. Pharmacother. 15 (2014) 1265–1276, https://doi.org/10.1517/14656566.2014.913024.
[48] L. Ma, J.R. Clayton, R.A. Walgren, B. Zhao, R.J. Evans, M.C. Smith, K.M. Heinz-Taheny, E.L. Kreklau, L. Bloem, C. Pitou, et al., Discovery and characterization of LY2784544, a small-molecule tyrosine kinase inhibitor of JAK2V617F, Blood Cancer J. 3 (2013) e109, https://doi.org/10.1038/bcj.2013.6.
[49] H. Xu, M.I. Jesson, U.I. Seneviratne, T.H. Lin, M.N. Sharif, L. Xue, C. Nguyen, R. A. Everley, J.I. Trujillo, D.S. Johnson, et al., PF-06651600, a dual JAK3/TEC family kinase inhibitor, ACS Chem. Biol. 14 (2019) 1235–1242, https://doi.org/10.1021/acschembio.9b00188.
[50] I.J. Kwon, S.E. Kim, S.C. Kim, S.E. Lee, Efficacy of oral JAK1 or JAK1/2 inhibitor for treating refractory pruritus in dystrophic epidermolysis bullosa: a retrospective case series, J. Dermatol. 51 (2024) 441–447, https://doi.org/10.1111/1346-8138.17079.
[51] X. Zhang, P. Yue, B.D. Page, T. Li, W. Zhao, A.T. Namanja, D. Paladino, J. Zhao, Y. Chen, P.T. Gunning, et al., Orally bioavailable small-molecule inhibitor of transcription factor Stat3 regresses human breast and lung cancer xenografts, Proc. Natl. Acad. Sci. U. S. A. 109 (2012) 9623–9628, https://doi.org/10.1073/pnas.1121606109.
[52] P. Yue, F. Lopez-Tapia, D. Paladino, Y. Li, C.H. Chen, A.T. Namanja, T. Hilliard, Y. Chen, M.A. Tius, J. Turkson, Hydroxamic acid and benzoic acid-based STAT3 inhibitors suppress human glioma and breast cancer phenotypes in vitro and in vivo, Cancer Res. 76 (2016) 652–663, https://doi.org/10.1158/0008-5472.CAN-14-3558.
[53] Schrödinger Release 2021–2, LigPrep, Schrödinger, LLC, New York, NY, USA, 2021.
[54] *Schrödinger Release 2021-2 : Protein Preparation Wizard*, Epik, Schrödinger, LLC, New York, NY, 2021. Impact, Schrödinger, LLC, New York, NY; Prime, Schrödinger, LLC, New York, NY, 2021.
[55] J.L. Banks, H.S. Beard, Y. Cao, A.E. Cho, W. Damm, R. Farid, A.K. Felts, T. A. Halgren, D.T. Mainz, J.R. Maple, et al., Integrated modeling program, applied chemical theory (IMPACT), J. Comput. Chem. 26 (2005) 1752–1780, https://doi.org/10.1002/jcc.20292.
[56] H.M. Berman, J. Westbrook, Z. Feng, G. Gilliland, T.N. Bhat, H. Weissig, I. N. Shindyalov, P.E. Bourne, The protein Data Bank, Nucleic Acids Res. 28 (2000) 235–242, https://doi.org/10.1093/nar/28.1.235.
[57] RCSB PDB, Available online: www.rcsb.org. (Accessed 29 June 2022).
[58] G.M. Sastry, M. Adzhigirey, T. Day, R. Annabhimoju, W. Sherman, Protein and ligand preparation: parameters, protocols, and influence on virtual screening enrichments, J. Comput. Aided Mol. Des. 27 (2013) 221–234, https://doi.org/10.1007/s10822-013-9644-8.
[59] W. Sherman, H.S. Beard, R. Farid, Use of an induced fit receptor structure in virtual screening, Chem. Biol. Drug Des. 67 (2006) 83–84, https://doi.org/10.1111/j.1747-0285.2005.00327.x.
[60] W. Sherman, T. Day, M.P. Jacobson, R.A. Friesner, R. Farid, Novel procedure for modeling ligand/receptor induced fit effects, J. Med. Chem. 49 (2006) 534–553, https://doi.org/10.1021/jm050540c.